Semiclassical wave packet study of ozone forming reaction

Evgeny Vetoshkin and Dmitri Babikov[a)]
Chemistry Department, Wehr Chemistry Building, Marquette University, Milwaukee, Wisconsin 53201-1881

(Received 14 March 2006; accepted 18 May 2006; published online 12 July 2006)

We have applied the semiclassical wave packet method (SWP) to calculate energies and lifetimes of the metastable states (scattering resonances) in a simplified model of the ozone forming reaction. All values of the total angular momentum up to $J=50$ were analyzed. The results are compared with numerically exact quantum mechanical wave packet propagation and with results of the time-independent WKB method. The wave functions for the metastable states in the region over the well are reproduced very accurately by the SWP; in the classically forbidden region and outside of the centrifugal barrier, the SWP wave functions are qualitatively correct. Prony's method was used to extract energies and lifetimes from the autocorrelation functions. Energies of the metastable states obtained using the SWP method are accurate to within 0.1 and 2 cm^{-1} for under-the-barrier and over-the-barrier states, respectively. The SWP lifetimes in the range of $0.5<\tau_n<100$ ps are accurate to within 10%. A three-level model was used to investigate accuracies of different approximations for the reaction rate constant. It was shown that the majority of the metastable states in this system are either long lived (narrow resonances) which can be treated as stable, or short lived (broad resonances) which can be treated without the knowledge of their lifetimes. Only a few metastable states fall into the intermediate range where both energies and lifetimes are needed to model the kinetics. The recombination rate constant calculated with the SWP method at room temperature and pressure is in good agreement with available experimental data. © *2006 American Institute of Physics*. [DOI: 10.1063/1.2213252]

I. INTRODUCTION

In Earth's stratosphere ozone (O_3) is formed from oxygen atoms and molecules as a product of the recombination reaction

$$O + O_2 + M \Rightarrow O_3 + M, \tag{1}$$

where M represents a "third body" that can be any atmospheric atom or molecule[1] able to carry away the excess energy, so that stable ozone molecules are produced. In stratospheric conditions, as well as in majority of laboratory studies,[2,3] this reaction is dominated by the Lindemann mechanism,[4] also known as the *energy transfer* (ET) mechanism:[5,6]

$$O + O_2 \underset{k^d}{\overset{k^f}{\rightleftarrows}} O_3^*, \tag{2}$$

$$O_3^* + M \xrightarrow{k^s} O_3 + M. \tag{3}$$

Here the first step accounts for the formation and decay of long-lived metastable species O_3^*; these can be viewed as quantum mechanical scattering resonances or as ozone molecules excited rotationally and vibrationally above the $O+O_2$ dissociation threshold. The second step describes collisional deactivation of these metastable O_3^* species to give stable O_3.

Despite the apparent simplicity of this process and the considerable amount of experimental[7–11] and theoretical[12–27] attention it has received in the last decade, the ozone formation reaction still remains a challenge to the chemical physics community. This is due to anomalously large isotope effects associated with this reaction that are not yet fully understood.[7,8,11,21] It has been demonstrated using quantum statistical (RRKM) theory first[13,15] that incorporation of *quantum zero-point energies* (ZPE) in reaction (2) is necessary to reproduce the intricate isotope dependence of ozone formation rates.[10] Quantum scattering calculations[20,21] have shown a large number of long-lived scattering resonances located in a very narrow ΔZPE energy range between the two (due to the isotope mass differences) dissociation thresholds. Population of these metastable O_3^* states builds up exclusively from the lower entrance channel and is stabilized very efficiently, which significantly enhances the formation rates through this channel and explains the anomalously large isotope effect. Classical trajectory simulations[25,26] were also able to give an isotope effect, but only when the potential energy surface (PES) in the channel regions is adjusted "by hand" to introduce the channel specific ΔZPE corrections.

Furthermore, for reaction (3), experimental evidence[10,28] of an isotope effect related to *quantum symmetry* has been found. This is supported by quantum scattering calculations on a simpler recombination reaction[29,30] where the symmetry of metastable states has been treated rigorously and found to

[a)]Author to whom correspondence should be addressed. Electronic mail: dmitri.babikov@mu.edu

produce an important isotope effect. It has also been shown that one can account for this effect by introducing (based on qualitative arguments related to difference in statistical density of states in symmetric and asymmetric O_3 isotopomers) a simple *ad hoc* correction factor into statistical[15] or classical trajectory[26] treatments and tuning this factor to fit the experimental results. Note that the metastable ozone states O_3^* play the central role in the isotope effects in both processes (2) and (3).

Although the progress in understanding the basic mechanisms of the isotope effect at a qualitative level has been impressive and we, perhaps, can say that the molecular origin of anomalous isotope effects has finally been identified, a quantitative theoretical treatment of the processes (2) and (3) is still lacking. It is fair to say that none of the existing theories of ozone formation reaction are both rigorous and complete: The RRKM-based theory,[15] apart from its statistical assumptions, lacks information about the ozone PES and involves an empirical treatment of symmetry. The classical trajectory method[26] is able to show the isotope effects only when these effects are expected and the desired quantum properties have been built into the classical formalism *a priori*. Such an approach cannot be regarded as based on the first principles. The quantum mechanical theories proposed so far are prohibitively expensive computationally and therefore either focused only on the first step (2) and thereby restricted to nonrotating (total angular momentum quantum number $J=0$) ozone molecules,[20,21] or limited by reduced dimensionality and sudden approximation assumptions for collision and vibration-rotation,[17] which are not valid for slow processes (2) and (3) where the relative motion of nuclei is rather adiabatic than sudden.

A theoretical method suitable for description of the isotope effects in (2) and (3) should account for all features of the complicated ozone PES,[19] incorporate full dimensionality of the problem, avoid using sudden approximations, be able to treat scattering resonances, and also include the quantum ZPE and quantum symmetry in a rigorous way. We think that the semiclassical wave packet (SWP) method, also known as the Herman-Kluk propagator[31–34] or as the initial value representation method,[35–37] might be a good approach for this problem. It takes into account all features of the PES in a natural, dynamic way; dimensionality of reactions (2) and (3) is not a problem for this trajectory-based method, and no sudden-type approximations are necessary. It is also well established that the SWP approach describes the quantum zero-point energy[37,38] and is able to reproduce quantum symmetry,[39] particularly the symmetry effects in state-to-state transitions in processes similar to the ozone forming reaction.[29]

Much less is known about the ability of the SWP approach to deal with quantum scattering resonances such as those in O_3^*. In the SWP study of collinear $H+H_2$ reactive scattering, significant oscillations in the state-to-state transition probabilities have been observed[40–42] and attributed to wide overlapping scattering resonances, but the resonances themselves were not characterized. In another study of collinear $H_3^* \rightarrow H+H_2$ decay,[43] the SWP method was used with particular emphasis on characterization of the scattering resonances and has been very successful. These are the only two examples we found in the literature. Unfortunately, the hydrogen exchange reaction is very different from our reaction (2) in two important ways. First, the nature of scattering resonances is quite different because the $H+H_2$ PES is purely repulsive with a relatively high transition state (4.75 eV), while the ozone PES exhibits no activation barrier and has a deep covalent bonding well (1.132 eV) and a shallow van der Waals well (209 cm^{-1}).[19] Second, the $H+H_2$ scattering is a high energy process (0.8–5 eV) observed in molecular beams, while our reaction (2) occurs at low stratospheric temperatures and the ΔZPE range, important for the isotope effects, is only about 30 cm^{-1} above the dissociation threshold.

Thus, it would be instructive to test the validity of the SWP approach on a simple problem relevant to the ozone forming reaction. We have carried out such a methodological study, and the results are reported in this paper. We applied the SWP method to describe quantum scattering resonances in an ozonelike two-body scattering system. We considered a simple model, where the internal structure of O_2 is neglected and the focus is on scattering resonances formed behind the centrifugal barrier due to the angular momentum of a relative $O+O_2$ motion. We took into account all values of J required to calculate the converged rate of ozone formation through the reactions (2) and (3) and characterized every important resonance by its energy and lifetime. Overall, we looked at more than 80 resonances with lifetimes (τ) that evenly cover the range from 0.01 to 1000 ps. This certainly represents a thorough test of the SWP approach. To assess its accuracy we compared the SWP results against the data obtained using a fully quantum wave packet propagation technique.[44] We also found it useful to compare the SWP results with results of another semiclassical method—the time-independent WKB.[45] General energetics of $O+O_2$ scattering is preserved in our model by using the ozone dissociation energy $D=1.132$ eV, its equilibrium distance $r_e=2.4$ a.u., and the $O-O_2$ reduced mass $\mu=\mu_{O-O_2}$ as parameters in the Morse potential function

$$V_J(r) = -D + D(1 - e^{-a(r-r_e)})^2 + \frac{\hbar^2 J(J+1)}{2\mu r^2}, \tag{4}$$

where r is the distance between colliding O and O_2 and the last term describes the centrifugal distortion.[46] The parameter $a=2.0$ was used to reproduce the dynamically important van der Waals part of the ozone PES in the channel region.[19] The frequency at the bottom of the potential well was reproduced only approximately, but this parameter is much less important for the recombination process. The potential function $V_J(r)$ for $J=38$ is shown in Fig. 1(a).

In Sec. II we briefly survey the time-dependent SWP method in order to introduce our notation. In Sec. III we apply the SWP method to obtain energies, lifetimes, and wave functions of the metastable states for potential (4). Section IV is devoted to the kinetics of reactions (2) and (3) and the calculation of the recombination rate. Conclusions are given in Sec. V.

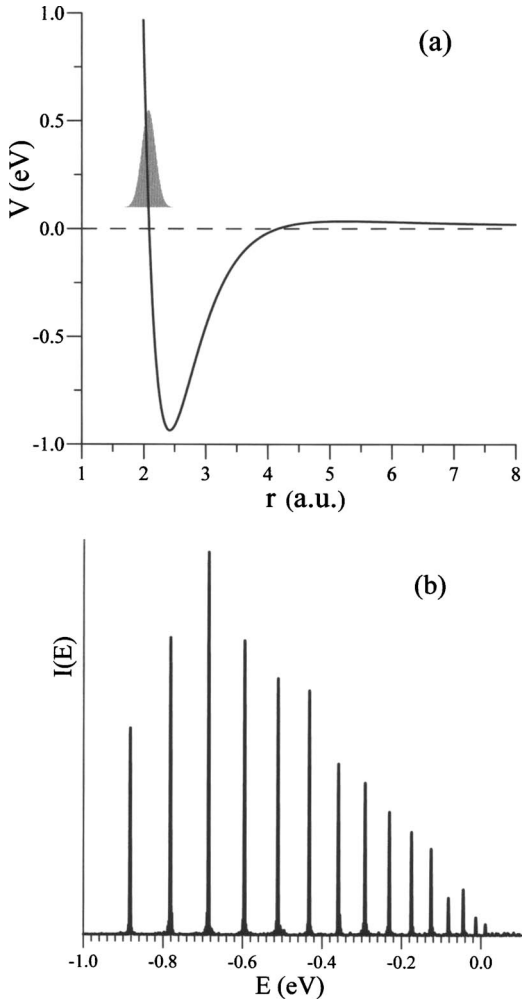

FIG. 1. (a) Initial wave packet with $\alpha=20$ and $p_0=0$ placed at the point $r_0=2.16$ a.u. on the potential function for $J=38$. (b) The half spectrum $I(E)$ calculated after SWP propagation of this initial wave packet through time $t_{\text{end}}=2.5$ ps with $N=10\,000$ classical trajectories and $\gamma=\alpha$.

II. SWP PROPAGATION

In the SWP method,[31,32] the time evolution of the wave function $\psi(r,t)$ of a quantum system is approximated by an integral over the initial phase space (r_i,p_i). For a one dimensional problem:

$$\psi(r,t)=\int \frac{dr_i dp_i}{2\pi\hbar}\langle\psi_\gamma(r',r_i,p_i)|\psi(r',0)\rangle\psi_\gamma(r,r_t,p_t) \times C(r_t,p_t,t)\exp\{iS(r_t,p_t,t)/\hbar\}. \quad (5)$$

Here, the initial wave function $\psi(r,0)$ is expanded in terms of an overcomplete set of N Gaussian functions of the form

$$\psi_\gamma(r,r_i,p_i)=\left(\frac{2\gamma}{\pi}\right)^{1/4}\exp\{-\gamma(r-r_i)^2+ip_i(r-r_i)/\hbar\} \quad (6)$$

placed at the various points (r_i,p_i) in the phase space and all characterized by the same width parameter γ. The expansion coefficients $\langle\psi_\gamma(r',r_i,p_i)|\psi(r',0)\rangle$ are computed only once. Each phase $S(r_t,p_t,t)$ in Eq. (5) represents the classical action

$$S(r_t,p_t,t)=\int_0^t[p_t^2/2\mu-V(r_t)]dt \quad (7)$$

accumulated along the classical trajectory that originates from the phase space point (r_i,p_i) at the initial moment of time and reaches the point (r_t,p_t) at time t. The prefactors $C(r_t,p_t,t)$ are computed as[33]

$$C(r_t,p_t,t)=\left|\frac{1}{2}\left(\frac{\partial p_t}{\partial p_i}+\frac{\partial r_t}{\partial r_i}-2\gamma i\hbar\frac{\partial r_t}{\partial p_i}+\frac{i}{2\gamma\hbar}\frac{\partial p_t}{\partial r_i}\right)\right|^{1/2}. \quad (8)$$

The N trajectories are propagated from (r_i,p_i) to (r_t,p_t) in a usual classical way:

$$\dot{r}_t=\frac{p_t}{\mu},\quad \dot{p}_t=-\left.\frac{dV(r)}{dr}\right|_{r=r_t}. \quad (9)$$

However, due to the phase factors $e^{iS/\hbar}$ in Eq. (5), these trajectories contribute to the semiclassical wave function of the system in a coherent way. All quantum mechanical effects arise as a result of this interference.

The initial points (r_i,p_i) are sampled using a Monte Carlo scheme based on the Box-Müller algorithm.[33] For simplicity the initial wave function $\psi(r,0)$ is chosen in the form of a Gaussian packet characterized by the width parameter α, average position r_0, and average momentum p_0:

$$\psi(r,0)=\psi_\alpha(r,r_0,p_0)=\left(\frac{2\alpha}{\pi}\right)^{1/4}\exp\{-\alpha(r-r_0)^2+ip_0(r-r_0)/\hbar\}. \quad (10)$$

In this case integration over r' in the expansion coefficients $\langle\psi_\gamma|\psi_\alpha\rangle$ can be carried out analytically, and the integral in Eq. (5) can be replaced with the sum

$$\psi(r,t)=\frac{1}{N}\frac{\sqrt{2(\alpha+\gamma)}}{(\alpha\gamma)^{1/4}}\sum_{i=1}^{N}\psi_\gamma(r,r_t,p_t)C(r_t,p_t,t) \times\exp\{i(S(r_t,p_t,t)+\delta(r_i,p_i))/\hbar\}, \quad (11)$$

where we have introduced

$$\delta(r_i,p_i)\equiv\frac{(r_i-r_0)(\alpha p_i+\gamma p_0)}{\alpha+\gamma}. \quad (12)$$

A practical application of the SWP method starts with choosing a suitable initial wave packet $\psi(r,0)$ defined by r_0, p_0, and α. Then, the initial phase space points (r_i,p_i) are randomly generated around (r_0,p_0) and are weighted by $\langle\psi_\gamma|\psi_\alpha\rangle$. For every initial point the two equations of motion (9), one equation for classical action (7), and four stability equations for $\partial p_t/\partial p_i$, $\partial r_t/\partial r_i$, $\partial r_t/\partial p_i$, $\partial p_t/\partial r_i$ [see Ref. 37] are numerically integrated through time t. The prefactors $C(r_t,p_t,t)$ are calculated from Eq. (8), taking care of square root branches. Finally, the wave packet $\psi(r,t)$ at time t is reconstructed according to Eqs. (11) and (12). The width of Gaussian functions γ and the number of trajectories N are used as convergence parameters. In the next section it is demonstrated that the autocorrelation function can also be calculated very efficiently using the SWP method.

III. SWP CHARACTERIZATION OF SCATTERING RESONANCES

The semiclassical wave function in Eq. (11) can be used to calculate the autocorrelation function

$$P(t) = \langle \psi(r,0) | \psi(r,t) \rangle \tag{13}$$

and the half spectrum

$$I(E) = \left| \int_0^\infty P(t) \exp\{iEt\} dt \right|^2. \tag{14}$$

The energy spectrum of potential (4) contains both bound and metastable states. The bound states are characterized by real negative energies $E_m < 0$ and real wave functions ϕ_m, while the metastable states are characterized by complex energies $E_n - i\Gamma_n/2$ with positive E_n and Γ_n and complex valued wave functions ϕ_n. Lifetimes of the metastable states are obtained as $\tau_n = \hbar/\Gamma_n$, and it is usually assumed that the metastable states can be distinguished from the nonresonant continuum states using the following condition:

$$\Gamma_n/2 \ll (E_n - E_{n-1}). \tag{15}$$

In practice the condition $\Gamma_n < (E_n - E_{n-1})$ is employed.

An arbitrary wave packet $\psi(r,t)$ can be expanded in terms of a complete set of functions, which includes both bound ϕ_m and metastable ϕ_n states:

$$\psi(r,t) = \sum_m c_m \phi_m(r) \exp\{-iE_m t\} + \sum_n c_n \phi_n(r) \exp\{-i(E_n - i\Gamma_n/2)t\}, \quad n \neq m. \tag{16}$$

Substituting (16) into (13) leads to

$$P(t) = \sum_m |c_m|^2 \exp\{-iE_m t\} + \sum_n |c_n|^2 \exp\{-i(E_n - i\Gamma_n/2)t\}. \tag{17}$$

By plugging (17) into (14) and using condition (15) to eliminate the cross terms we obtain

$$I(E) \approx \pi^2 \sum_m |c_m|^4 \delta(E - E_m) + \sum_n |c_n|^4 \frac{1}{(\Gamma_n/2)^2 + (E - E_n)^2}. \tag{18}$$

Here $\delta(E - E_m)$ is the Dirac delta function. Expression (18) indicates that the half spectrum should exhibit a set of delta functions for the bound states and a set of Lorentzians for the metastable states. Using this knowledge, one can determine E_m, E_n, and Γ_n by analyzing the shape of $I(E)$. This can be done for isolated (nonoverlapping) scattering resonances by fitting each single peak with the Lorentzian function using E_n and Γ_n as tuning parameters.[43,47] From (16) it also follows that complex wave functions $\phi_n(r)$ of the metastable states can be found to within a normalization factor:

$$\phi_n(r) \approx \int_0^\infty \psi(r,t) \exp\{iE_n t\} dt. \tag{19}$$

Here the condition (15) has also been used.

When we use the SWP expression (11) for propagation of the wave packet $\psi(r,t)$, the integral in Eq. (13) splits onto N overlap integrals between the Gaussian functions $\psi_\gamma(r, r_t, p_t)$ and the initial wave packet $\psi_\alpha(r, r_0, p_0)$. These integrals can be calculated analytically, and the autocorrelation function at every time step can be computed simply as

$$P(t) = \frac{2}{N} \sum_{i=1}^{N} C(r_t, p_t, t) \exp\{i(S(r_t, p_t, t) + \delta(r_i, p_i) - \delta(r_t, p_t))/\hbar\} \times \exp\left[-\frac{\alpha\gamma}{(\alpha+\gamma)} (r_t - r_0)^2 - \frac{1}{4\hbar^2(\alpha+\gamma)} (p_t - p_0)^2 \right]. \tag{20}$$

Thus, in the SWP method, the autocorrelation function can be obtained in a very efficient way, without explicit reconstruction of the time-dependent wave packet $\psi(r,t)$.

Figure 1(b) gives the half spectrum $I(E)$ obtained using the SWP approach for our model system (4) at $J=38$. The initial wave packet with $\alpha=20$ was placed at $r_0=2.16$ a.u. with $p_0=0$, as shown in Fig. 1(a). In this case 10 000 randomly generated Gaussian functions with $\gamma=\alpha$ were used for the SWP expansion and the 10 000 classical trajectories were propagated over a time of $t_{end}=2.5$ ps. Since in practice the propagation time is always finite, the infinite integration limit in Eq. (14) should be, strictly speaking, replaced with this finite propagation time t_{end}. This would transform the delta functions in the half spectrum of Eq. (18) into sharp spikes with certain (small) widths. It also follows from Eq. (18) that the amplitudes of these spikes are determined by the overlap factors c_m. These properties are clearly reflected in Fig. 1(b). Fourteen spikes at $E<0$ correspond to the bound states in this potential. The amplitudes of the spikes change smoothly, with $v=2$ being the most intense and the three upper states $v=11$, 12, and 13 being less intense. All the bound states, starting from the ground vibrational state $v=0$ and up to the last bound state $v=13$, are reproduced quite well. It is interesting that a single SWP is able to capture all the bound states of the system. We found that a wide enough initial packet centered in the well or one shifted towards the repulsive wall covers the wide energy range and often contains the full spectrum of bound states. One metastable state ($v=14$) can also be seen in Fig. 1(b) as a small peak at $E>0$. Apparently, its overlap with the initial wave packet is insufficient for an accurate characterization of this and especially higher-lying metastable states.

Thus, an important factor for success of the time-dependent approach is a meaningful choice of the initial wave packet. For an accurate description of the scattering resonances we must choose a wave packet that covers a narrow energy range of interest and overlaps significantly with all the important metastable states. Also, it would be nice to have a general recipe applicable to the wide range of J values. After trying different possibilities we concluded that a

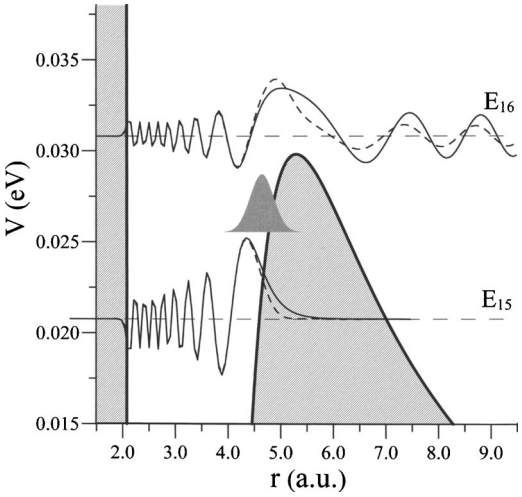

FIG. 2. Barrier region of the $J=38$ potential function. Initial wave packet with $\alpha=10$ and $p_0=0$ is placed at $r_0=4.64$ a.u. Wave functions of under-the-barrier ($v=15$) and over-the-barrier ($v=16$) metastable states were calculated by propagating this initial wave packet and then using Eq. (19). Solid line-quantum propagation; dashed line-SWP propagation with $\gamma=\alpha=10$ and $N=10\,000$. Shaded areas show the classically forbidden regions; the barrier top is at $r_{\text{top}}=5.29$ a.u.

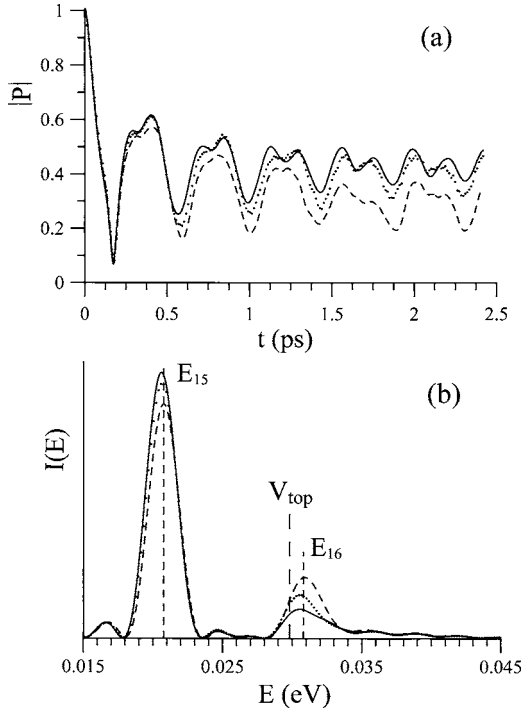

FIG. 3. (a) The autocorrelation function and (b) the half spectrum obtained from propagation of the initial wave packet shown in Fig. 2. Solid line-quantum propagation; dashed line-SWP propagation with $\gamma=\alpha=10$ and $N=10\,000$. Dotted line-SWP propagation with very small $\gamma=0.6$ and very large $N=500\,000$; see text for details. Vertical lines in frame (b) show energy of the barrier top (V_{top}) and energies of two metastable states ($v=15$ and $v=16$) extracted from the autocorrelation function using the Prony analysis at time $t_{\text{end}}=1.45$ ps.

simple and robust rule is to place the initial packet on the internal slope of the centrifugal barrier where the potential changes less rapidly, as shown in Fig. 2, slightly shifted to the left from the barrier top. This rule is rationalized by the fact that the wave functions of the metastable states exhibit a wide maximum in this region (see Fig. 2), so that the overlap coefficients c_n are usually large for all states of interest. We also found that the width of the initial wave packet with $\alpha=10$ is enough to capture all the metastable states of interest for all necessary values of J, making only insignificant overlaps with the continuum or the bound states.

Using this protocol, in Fig. 2 we show the barrier region of the same $J=38$ potential function shown in Fig. 1(a), but now the wave packet with $\alpha=10$ and $p_0=0$ was placed at $r_0=4.64$ a.u. and propagated using the SWP method with 10 000 trajectories and $\gamma=\alpha$ as in the previous example. For the purpose of comparison we also propagated this initial wave packet using the numerically accurate quantum method,[44] and the results are shown in Fig. 3. During the first 0.55 ps the $|P(t)|$ drops from 1 to a small value, rises back to a maximum with $|P(t)|\sim 0.6$, and drops again to a second minimum. This part of dynamics is reproduced very accurately by the SWP method [see Fig. 3(a)]. After 0.55 ps the difference between the quantum and SWP values of $|P(t)|$ increases, but the general oscillatory behavior of $|P(t)|$ is still reproduced quite well by the SWP method, and this is sufficient for characterization of most of the metastable states of interest. Note: on a one-processor computer the SWP propagation with 10 000 trajectories was a factor of 8 faster than the full quantum propagation. Furthermore, computational scaling of the SWP method on a parallel machine should be nearly perfect because independent classical trajectories can be propagated on different processors without any message passing during the propagation time.

We found two important reasons why the SWP value of $|P(t)|$ is smaller than the quantum one. First, the norm of SWP wave functions is not accurately preserved. For example, at the end of time interval shown in Fig. 3(a) it fluctuates around the value of $|\psi(r,t)|^2\sim 0.75$. Simply renormalizing the SWP wave function at every time step before the autocorrelation function is computed accounts for 20%–70% of errors in $|P(t)|$. The second reason is relevant to the SWP description of tunneling. It is well known that, when the spectrum of the initial wave packet contains only the bound states, the SWP autocorrelation function is almost identical to the quantum one. We have confirmed this in our calculations (Fig. 1, for example). The discrepancies, such as those in Fig. 3(a), are observed only when metastable states are present in the spectrum of the packet. To eliminate this discrepancy, the mechanism by which quantum tunneling is described in the trajectory-based SWP method must be understood. It is intuitively clear that if we use very narrow Gaussian functions ($\gamma\to\infty$), the range of r_i's sampled with classical trajectories at $t=0$ would be equal to the width of the initial wave packet $\psi_\alpha(r,r_0,p_0)$ determined by α. All such trajectories (see Fig. 2) would remain trapped in the well forever and reproduce no tunneling at all. However, when the initial phase space is sampled with the Gaussian functions $\psi_\gamma(r,r_i,p_i)$ of finite width, the range of r_i covered by the sampling procedure is determined not only by α but also by γ, since all points r_i with nonzero overlap $\langle\psi_\gamma|\psi_\alpha\rangle$ should be sampled and the overlap is determined by both α and γ (actually, in the equal sense). For example, when we

took $\gamma=\alpha=10$ the range sampled at $t=0$ was $3.1<r_i<6.0$ a.u., which is twice the width of the initial wave packet determined by α (see Fig. 2). Such a sampling gives some trajectories (in this case only 2% of the total) that start on the outside slope of the barrier, "explore" that part of PES, and, finally, leave. Those trajectories are responsible for a description of tunneling in the SWP method, and we should try to increase their number for better accuracy. [Simply increasing the total number of trajectories N does not help. Increasing the width of the initial wave packet (by changing α) is not convenient because the spectrum and the autocorrelation function become very complicated.] This could be done by increasing the widths of the Gaussian functions $\psi_\gamma(r,r_i,p_i)$, which in turn would lead to sampling of a wider range of r_i's. Doing so better reproduces tunneling, but produces a noisy autocorrelation function because now a much wider range of space is sampled using the same number of trajectories, and therefore evolution of the wave function is not described as accurately as before. Simply increasing the number of trajectories reduces such noise. Thus, γ and N are not truly independent parameters in the SWP method; i.e., when γ is reduced the number of trajectories N must be increased. We have repeated the SWP calculations for $\alpha=10$ using different γ and N, and our results confirm this explanation. As a limiting case the width parameter was reduced to $\gamma=0.6$ and the number of trajectories was increased to $N=500\,000$, leading to a wide range of $0.15<r_i<8.8$ a.u. being sampled by classical trajectories at $t=0$ and 25% of the trajectories being initially at points outside of the barrier. In this run the quantum dynamics was reproduced accurately through the entire range of 2.5 ps [see Fig. 3(a), dotted line] and even longer. Thus, the accuracy of SWP propagation can be improved at the expense of computational effort (determined by N).

In Fig. 3(b) the calculated SWP half spectrum $I(E)$ is presented and compared with the quantum result. The spectrum is dominated by two peaks at 0.0207 and 0.0309 eV. The first (sharper) peak is surrounded by some "noise" due to the finite propagation time. This peak is located substantially below the top of the centrifugal barrier V_{top}; such metastable states are usually longer lived and will be called *under-the-barrier* states hereafter. The energy of the second peak is slightly above the V_{top}, and this peak is broader. Such metastable states are usually shorter lived and will be called *over-the-barrier* states. The reader may also note a series of broad overlapping peaks forming a wavy structure in the high energy part of the spectrum. Analysis shows that these peaks are characterized by large $\Gamma_n>(E_n-E_{n-1})/2$ and should not be regarded as a progression of the metastable states, but rather a gradual transition to continuum. Note: The SWP method reproduces all these features of the half spectrum. Small discrepancies in positions, intensities, and shapes of the peaks do exist (and will be characterized below in terms of E_n and Γ_n), but, if necessary, the accuracy of the SWP method can be improved by increasing the number of dissociative trajectories as described above.

Equation (18) shows that the values of E_n and Γ_n can be extracted from $I(E)$ by fitting each peak in the half spectrum with a Lorentzian function. However, this is not very accurate at finite propagation times when the peaks are not yet Lorentzians [see Fig. 3(b)]. Also, it is not very practical when the characterization of many resonances is needed. An alternative approach, based on Eq. (17), is to fit the entire autocorrelation function $P(t)$ with a function of the form

$$P(t)=\sum_{n=1}^{L} b_n \exp\{-i(E_n-i\Gamma_n/2)t\}. \tag{21}$$

This approach allows extracting accurate E_n's and Γ_n's at relatively short propagation times, when errors in the semiclassical wave packets are insignificant. In the Prony algorithm[48–50] the $P(t)$ function is defined on a regular grid of $2L$ points and the unknown coefficients b_n, E_n, and Γ_n are determined using a least-squares nonlinear method. A disadvantage of this method is the occurrence of false resonances when large values of L are used for representation of $P(t)$. However, the true resonances can be easily identified by large real factors b_n and also by stable values of E_n and Γ_n with respect to variations of L.

Using the Prony algorithm, the energies and lifetimes were extracted from the SWP and quantum mechanical autocorrelation functions, and these are presented in Table I. The deviation in SWP energies of the metastable states seen in Fig. 3(b) are only 0.03 and 1.8 cm^{-1} for under-the-barrier and over-the-barrier states, respectively. This accuracy is typical for other metastable states over a wide range of J values (see Table I) which represents a remarkable success of the SWP method. For the metastable states with lifetimes in the range of $0.5<\tau_n<100$ ps, i.e., when the resonances are not too narrow and not too broad ($5\times10^{-6}<\Gamma_n<10^{-3}$ eV), the SWP predictions of Γ_n's are accurate to within 10%. They are still semiquantitatively correct (accurate to within 50%) for short-lived metastable states with $\tau_n<0.5$ ps ($\Gamma_n>10^{-3}$ eV). This lifetime range is much harder to analyze, even using the Prony algorithm, due to multiple overlaps of very wide resonances. We also found that on the other edge of the lifetime spectrum ($\tau_n>100$ ps) the accuracy of the SWP method is limited to roughly 5×10^{-6} eV and the widths of very narrow ($\Gamma_n<5\times10^{-6}$ eV) resonances cannot be accurately calculated. However, as described in the next section, the lifetimes of very narrow and very broad resonances play only a minor role in the recombination process.

The results obtained using the time-independent semiclassical WKB method are also presented in Table I. In the present implementation, the standard WKB method is improved[45] to treat the metastable states near and slightly above the barrier top. On average, the accuracy of the two semiclassical methods is roughly the same. A further comparison of SWP, WKB, and quantum results is available for download from EPAPS,[51] which includes the analysis of all scattering resonances in this system.

Finally, the wave functions for the two metastable states identified in the half spectrum of Fig. 3(b) were calculated using Eq. (19). Their real parts are shown in Fig. 2, which demonstrates that within the well region the SWP wave functions are in very good agreement with quantum wave functions. Inspection of the nodal structure allows us to assign the under-the-barrier resonance very clearly as the $v=15$ state. The next, over-the-barrier wave function has 16 nodes

TABLE I. Energies and lifetimes of the metastable states in potential (4) calculated via Prony analysis of the autocorrelation function found from the semiclassical (SWP) and quantum (QM) propagation of wave packets. Values designated as WKB has been calculated with traditional semiclassical time-independent WKB method.

		E_n (eV)				Γ_n (eV)			
J	n	SWP	WKB	QM	$E_{SWP}-E_{WKB}, E_{SWP}-E_{QM}$	SWP	WKB	QM	$\Gamma_{SWP}-\Gamma_{WKB}, \Gamma_{SWP}-\Gamma_{QM}$
8	19	0.000 53	0.000 51	0.000 47	$2.0\times10^{-5}, 6.0\times10^{-5}$	2.6×10^{-5}	1.5×10^{-5}	2.8×10^{-5}	$1.1\times10^{-5}, -0.2\times10^{-5}$
16	18	0.001 89	0.001 87	0.001 84	$2.0\times10^{-5}, 5.0\times10^{-5}$	$<5.0\times10^{-6}$	3.1×10^{-8}	8.3×10^{-9}	$<5.0\times10^{-6}, <5.0\times10^{-6}$
16	19[a]	0.005 76	0.005 41	0.005 20	$3.5\times10^{-4}, 5.6\times10^{-4}$	4.1×10^{-3}	5.8×10^{-3}	8.4×10^{-3}	$-1.7\times10^{-3}, -4.3\times10^{-3}$
17	18	0.002 84	0.002 98	0.002 93	$-1.4\times10^{-4}, -9.0\times10^{-5}$	5.5×10^{-6}	2.3×10^{-6}	2.2×10^{-6}	$3.2\times10^{-6}, 3.3\times10^{-6}$
18	18	0.004 09	0.004 11	0.004 01	$-2.0\times10^{-5}, 8.0\times10^{-5}$	3.2×10^{-5}	3.0×10^{-5}	3.5×10^{-5}	$0.2\times10^{-5}, -0.3\times10^{-5}$
19	18	0.005 19	0.005 25	0.005 14	$-6.0\times10^{-5}, 5.0\times10^{-5}$	1.5×10^{-4}	1.5×10^{-4}	1.7×10^{-4}	$0.06\times10^{-4}, -0.2\times10^{-4}$
20	18	0.006 35	0.006 35	0.006 26	$4.0\times10^{-6}, 9.0\times10^{-5}$	2.9×10^{-4}	3.4×10^{-4}	2.8×10^{-4}	$-0.5\times10^{-4}, 0.1\times10^{-4}$
21	18[a]	0.007 55	0.007 42	0.007 39	$1.3\times10^{-4}, 1.6\times10^{-4}$	6.0×10^{-4}	5.4×10^{-4}	5.9×10^{-4}	$0.6\times10^{-4}, 0.1\times10^{-4}$
22	18[a]	0.008 75	0.008 69	0.008 58	$6.0\times10^{-5}, 1.7\times10^{-4}$	1.4×10^{-3}	1.3×10^{-3}	1.4×10^{-3}	$0.1\times10^{-3}, 0.05\times10^{-3}$
23	17	0.004 13	0.004 09	0.004 06	$4.0\times10^{-5}, 7.0\times10^{-5}$	$<5.0\times10^{-6}$	8.1×10^{-11}	$<10^{-9}$	$<5.0\times10^{-6}, <5.0\times10^{-6}$
23	18[a]	0.010 68	0.010 12	0.010 59	$5.6\times10^{-4}, 9.0\times10^{-5}$	1.6×10^{-3}	2.6×10^{-3}	3.0×10^{-3}	$-1.0\times10^{-3}, -1.4\times10^{-3}$
24	17	0.006 02	0.005 99	0.005 95	$3.0\times10^{-5}, 7.0\times10^{-5}$	$<5.0\times10^{-6}$	2.6×10^{-8}	2.1×10^{-8}	$<5.0\times10^{-6}, <5.0\times10^{-6}$
24	18[a]	0.011 26	0.011 68	0.011 40	$-4.2\times10^{-4}, -1.4\times10^{-4}$	4.2×10^{-3}	4.3×10^{-3}	7.9×10^{-3}	$-0.1\times10^{-3}, -3.7\times10^{-3}$
31	17[a]	0.020 26	0.019 55	0.019 48	$7.1\times10^{-4}, 7.8\times10^{-4}$	3.1×10^{-3}	2.5×10^{-3}	3.2×10^{-3}	$0.6\times10^{-3}, 0.1\times10^{-3}$
35	16	0.022 93	0.022 86	0.022 69	$7.0\times10^{-5}, 2.4\times10^{-4}$	1.7×10^{-4}	1.6×10^{-4}	1.3×10^{-4}	$0.1\times10^{-4}, 0.4\times10^{-4}$
38	15	0.020 70	0.020 76	0.020 70	$-6.0\times10^{-5}, -4.0\times10^{-6}$	$<5.0\times10^{-6}$	6.0×10^{-9}	5.8×10^{-9}	$<5.0\times10^{-6}, <5.0\times10^{-6}$
38	16[a]	0.030 90	0.030 80	0.030 68	$1.0\times10^{-4}, 2.2\times10^{-4}$	1.6×10^{-3}	1.9×10^{-3}	1.7×10^{-3}	$-0.3\times10^{-3}, -0.1\times10^{-3}$

[a]Over-the-barrier state.

in the well region. Its real and imaginary parts exhibit more oscillations in front of the barrier, but these cancel when the modulus of the wave function is calculated, so that $|\psi(r)|$ shows only 16 nodes and a long tail with a gradually decreasing amplitude (not shown in Fig. 2). Thus, this metastable state can be assigned as $v=16$. Some quantitative differences are seen outside of the main well, where the SWP wave functions die off faster than quantum wave functions. For the $v=15$ state this discrepancy occurs in the classically forbidden region, while for the $v=16$ state this is seen in the barrier region and further on the left side of the barrier. These discrepancies are certainly due to the semiclassical approximation which is able to reproduce quantum tunneling only approximately.

IV. KINETICS OF OZONE FORMATION

To describe the kinetics of ozone formation we introduce rate coefficients for the processes of formation, decay, and stabilization of the metastable O_3^*: k^f, k^d, and k^s, respectively, as shown in Eqs. (2) and (3). Assuming steady state conditions for the concentration of the metastable O_3^* and introducing the equilibrium constant $K=k^f/k^d$ for reaction (2) we obtain the well known expression for the rate of the recombination process:[3,18]

$$\frac{d[O_3]}{dt}=\kappa[O][O_2][M], \tag{22}$$

$$\kappa\equiv K\frac{k^d k^s}{k^d+k^s[M]}. \tag{23}$$

Here κ represents the third order reaction rate coefficient for the entire reaction (1). It is instructive to consider two limiting cases where the expression (23) can be simplified:

$$k^d \ll k^s[M]: \quad \kappa=K\frac{k^d}{[M]}; \tag{24}$$

$$k^d \gg k^s[M]: \quad \kappa=Kk^s. \tag{25}$$

As expected, in either case the rate of the entire reaction (1) is determined by the rate limiting (slower) step. The first limit describes a situation in which the metastable O_3^* are stabilized very efficiently, but they form (and decay) very slowly. Decay of the metastable O_3^* species is a first order kinetic process characterized simply by their lifetime:

$$k^d=\Gamma. \tag{26}$$

Thus, the limiting case (24) is achieved when $\Gamma \ll k^s[M]$, i.e., when the scattering resonances are narrow and the metastable states are long lived. On the contrary, the limit (25) is achieved when $\Gamma \gg k^s[M]$, i.e., when the scattering resonances are broad and the metastable states are short lived. Indeed, Eq. (25) describes the case where the process of formation (and decay) of the metastable O_3^* is fast compared to stabilization. As in several earlier studies,[20,21] we adopt the *exponential down* model[52] and calculate the stabilization rate coefficient as

$$k^s=\omega(T)\exp\left\{-\frac{E-E_0}{\Delta E}\right\}, \tag{27}$$

where $\omega(T)$ is the temperature dependent Lennard-Jones collision frequency for O_3^*+M collisions.[13,53] Energies of the metastable O_3^* and stable O_3 species enter this expression as E and E_0, respectively; the parameter ΔE represents the average energy removed from O_3^* per one collision with M.[52]

It is important to emphasize that in the first limit the recombination rate coefficient κ is determined solely by the lifetime Γ of the metastable O_3^*, while in the second limit κ is

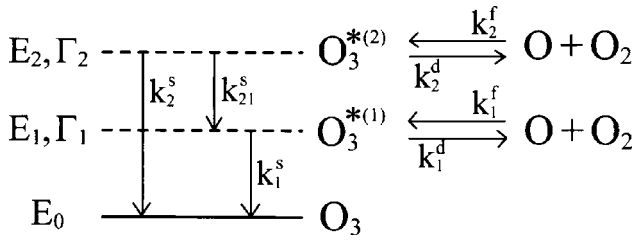

FIG. 4. Diagram of the energy transfer mechanism in a three-level system. Two metastable states $O_3^{*(1)}$ and $O_3^{*(2)}$ with energies and width (E_1, Γ_1) and (E_2, Γ_2), respectively, are stabilized by third body collisions to give stable O_3 in the bound state at energy E_0. Stabilization rate coefficients are k_1^s, k_2^s, and k_{21}^s. The rates of formation and decay of the metastable states are determined by k_1^f, k_2^f, k_1^d, and k_2^d.

determined exclusively by the excitation energy E of the metastable O_3^*. Only in the intermediate regime, when $k^d \sim k^s[M]$, are the values of Γ and E both important and the reaction rate coefficient κ then must be calculated from the general expression (23). Furthermore, if we theoretically "clamp" the energy E of the metastable O_3^* and vary only its lifetime Γ in a wide range, we see that in the first limit the reaction rate coefficient κ is small, while in the second limit it reaches its maximum value $\kappa = Kk^s$.

In the previous section we have demonstrated that the energies and especially lifetimes of the metastable ozone states vary widely. Thus, special care should be taken, and the validity of one or another approximation should be determined before applying either formula (24) or (25). Furthermore, since more than one metastable state can be involved in the recombination process, even the general expression (23) may not always be appropriate. For example, Fig. 4 represents a recombination process that involves two metastable states denoted as $O_3^{*(1)}$ and $O_3^{*(2)}$ characterized by their formation and decay rates: k_1^f, k_2^f, k_1^d, and k_2^d. Stabilization of both metastable states into the upper stable O_3 state should be considered and described by k_1^s and k_2^s, so does the intermediate stabilization step $O_3^{*(2)} \rightarrow O_3^{*(1)}$ described by k_{21}^s. The rate of ozone formation is then expressed as

$$\frac{d[O_3]}{dt} = (k_1^s[O_3^{*(1)}] + k_2^s[O_3^{*(2)}])[M]. \tag{28}$$

Master equations for the concentrations of the metastable states are

$$\frac{d[O_3^{*(1)}]}{dt} = k_1^f[O][O_2] - k_1^d[O_3^{*(1)}] + (k_{21}^s[O_3^{*(2)}] - k_1^s[O_3^{*(1)}])[M], \tag{29}$$

$$\frac{d[O_3^{*(2)}]}{dt} = k_2^f[O][O_2] - k_2^d[O_3^{*(2)}] - (k_{21}^s + k_2^s)[O_3^{*(2)}][M]. \tag{30}$$

Assuming the steady state conditions for both states,

$$\frac{d[O_3^{*(i)}]}{dt} \approx 0, \quad i = \{1,2\}, \tag{31}$$

and introducing the equilibrium constants

$$K_i = \frac{k_i^f}{k_i^d}, \quad i = \{1,2\}, \tag{32}$$

we obtain from Eqs. (28)–(31), an expression equivalent to Eq. (22), but with the third order recombination rate coefficient in the following form:

$$\kappa = K_1 \frac{k_1^d k_1^s}{k_1^d + k_1^s[M]} + K_2 \frac{k_2^d\{k_{21}^s k_1^s[M] + k_2^s(k_1^d + k_1^s[M])\}}{\{k_1^d + k_1^s[M]\}\{k_2^d + (k_2^s + k_{21}^s)[M]\}}. \tag{33}$$

Here, the rate coefficients of elementary processes are determined by the energies and lifetimes of two metastable states:

$$k_i^d = \Gamma_i, \quad i = \{1,2\}, \tag{34}$$

$$k_i^s = \omega(T)\exp\left\{-\frac{E_i - E_0}{\Delta E}\right\}, \quad i = \{1,2\}, \tag{35}$$

$$k_{21}^s = \omega(T)\exp\left\{-\frac{E_2 - E_1}{\Delta E}\right\}. \tag{36}$$

We found this mechanism appropriate for description of the recombination process in our $O+O_2$ model system; it was also very useful for understanding the recombination kinetics and allowed us to draw some general conclusions applicable to the recombination processes that involve more than two metastable states.

First, let us consider two extreme cases of Eq. (33), when both metastable states are either narrow or broad. From Eq. (33) we obtain

$$k_1^d \ll k_1^s[M], \quad k_2^d \ll k_{21}^s[M]: \quad \kappa = K_1\frac{k_1^d}{[M]} + K_2\frac{k_2^d}{[M]}; \tag{37}$$

$$k_1^d \gg k_1^s[M], \quad k_2^d \gg k_{21}^s[M]: \quad \kappa = K_1 k_1^s + K_2 k_2^s. \tag{38}$$

Comparing these expressions with Eqs. (24) and (25), we can conclude that in these limiting cases, different metastable states contribute independently to the total recombination rate.

Formula (37) can be further simplified. In the previous section we saw that the lifetimes of narrow (under-the-barrier) states decrease very rapidly when energy increases, and for any two consecutive narrow states $O_3^{*(1)}$ and $O_3^{*(2)}$ the condition $\Gamma_1 \ll \Gamma_2$ is usually satisfied by at least an order of magnitude. This allows us to neglect the first term in Eq. (37) and obtain $\kappa \approx K_2\Gamma_2/[M]$, equivalent to Eq. (24), which simply means that a very narrow metastable state contributes very little to the recombination rate and can rather be considered as an upper bound state. Thus, the limiting case presented in Eq. (37) is somewhat artificial: there is never a reason to take into account more then one narrow under-the-barrier state; in some circumstances the last (upper) narrow state should still be considered as metastable, but the state below it can always be considered as an upper bound state.

The second limit [Eq. (38)] can be easily generalized to describe the case of an arbitrary number of broad metastable states:

$$\Gamma_i \gg k^s_{i,(i-1)}[M]: \quad \kappa = \sum_i K_i k^s_i. \tag{39}$$

In this sum, each term is substantially smaller then the previous one due to the exponential dependence of k^s_i on E_i in formula (35). Thus, the sum in Eq. (38) should quickly converge with the major contribution from the first term (i.e., from the lowest broad metastable state).

Another useful limit of Eq. (33) is obtained if the first metastable state $O_3^{*(1)}$ is assumed to be narrow, but the second metastable state is kept in the general form. For such a case we obtain the following from (33):

$$k^d_1 \ll k^s_1[M]: \quad \kappa = K_1 \frac{k^d_1}{[M]} + K_2 \frac{k^d_2(k^s_2 + k^s_{21})}{k^d_2 + (k^s_2 + k^s_{21})[M]}. \tag{40}$$

Comparing this result with expressions (23), (24), and (37), we can tell that although an additional stabilization pathway (k^s_{21}) is now available for the second state $O_3^{*(2)}$, the contributions from two states are still quite independent. Furthermore, when the spectrum of the metastable states is not very dense, it is usually true that $k^s_2 \ll k^s_{21}$ [see Eqs. (35) and (36)], and from (40) we obtain

$$k^d_1 \ll k^s_1[M], \quad k^s_2 \ll k^s_{21}: \quad \kappa = K_1 \frac{k^d_1}{[M]} + K_2 \frac{k^d_2 k^s_{21}}{k^d_2 + k^s_{21}[M]}. \tag{41}$$

Now the contributions of states $O_3^{*(1)}$ and $O_3^{*(2)}$ are indeed independent. Also, since here the first state is narrow and the second is not, the condition $\Gamma_1 \ll \Gamma_2$ is satisfied and we can neglect the first term in Eq. (41), which leads us to an equation equivalent to Eq. (23):

$$k^d_1 \ll k^s_1[M], \quad k^s_2 \ll k^s_{21}: \quad \kappa \approx K_2 \frac{k^d_2 k^s_{21}}{k^d_2 + k^s_{21}[M]}. \tag{42}$$

This means that when there is (in the spectrum) a metastable state which is *not* narrow, all the narrow metastable states below it can be treated simply as bound because their contributions are, anyway, very small compared to the contribution of that not narrow state.

Based on these considerations, we developed a simple procedure for an analysis of the metastable states. First, we identify all narrow metastable states using the following criterion:

$$\Gamma_i \ll k^s_{i,(i-1)}[M], \tag{43}$$

and simply treat these as bound states. In our case the error due to this approximation is less than (minus) 1% of the value of κ. Then, using the opposite criterion (39), we could identify all the broad states and calculate their contributions using Eq. (38). Note: to use Eq. (38) we need to know only the energies E_i of the metastable states; the knowledge of accurate lifetimes Γ_i is not required. Due to this approximation, the error in κ is only about (plus) 1%. The remaining states should be treated in a general way, but the point is that at any value of J there will be just one or at most two such metastable states, and we can then apply our mechanism (Fig. 4) and use expression (33).

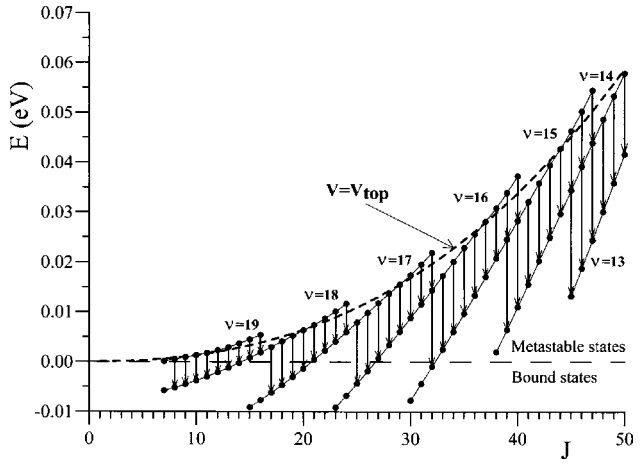

FIG. 5. Energies of several upper states in the model system of Eq. (4) for the $O+O_2$ collision. The dashed line shows energy of the barrier top (V_{top}) as a function of J. At $J<8$ there are no metastable states; as J increases, more and more metastable states appear. The majority of states are under-the-barrier states, but some over-the-barrier states are also present. States are labeled by the vibrational quantum number v. For each value of J the transition is shown (by arrow) from the *not* narrow metastable states to the upper bound state, or to the upper narrow metastable state, when present. See text for details.

In Fig. 5 we summarize characteristics of the metastable states in our $O+O_2$ model system [Eq. (4)]. For $J<8$ we found no states that satisfy condition (15). As J increases, the energy of the barrier top rises (shown as V_{top}) but the number of states decreases, reflecting a faster decrease in the well depth. As described above, we first identified states that are narrow according to criterion (42). All such states are under-the-barrier states. Then, for each value of J, we plotted only transitions from the not narrow (truly metastable) states into the upper bound state, or into the upper narrow (almost bound) metastable state when such a state is present (see Fig. 5). We found that only in six cases, $J=32$, 39, 40, 45, 46, and 47, are there two not narrow metastable states which should be treated using Eq. (33). For the majority of J values there is only one not narrow metastable state left which can be treated using Eq. (41). In fact, in such simple cases we could slightly relax criterion (42) and, for every such J, also consider one narrow metastable state (the upper one) and treat those using the two-state formula (40) or (39), or even the general expression (33).

Thus, for our $O+O_2$ model system, there is no real need to verify whether or not the metastable resonances are wide according to the criterion in (38). However, the expression (38) for κ might be useful in some circumstances because it is simple and especially because it does not require the knowledge of accurate Γ_i's. Therefore, we have analyzed widths of all not narrow resonances shown in Fig. 5; the results are presented in Fig. 6. Two dashed lines divide the frame of Fig. 6 onto three areas. In the area above the upper dashed line the condition $\Gamma_i \gg k^s_{i,(i-1)}[M]$ holds and the readers can see that majority of the resonances fall into this region (i.e., they are broad). We found that all over-the-barrier states and many under-the-barrier states are broad. Only six resonances with $J=17$, 25, 32, 39, 45, and 46 fall within the area between the dashed curves, where $\Gamma_i \sim k^s_{i,(i-1)}[M]$, i.e.,

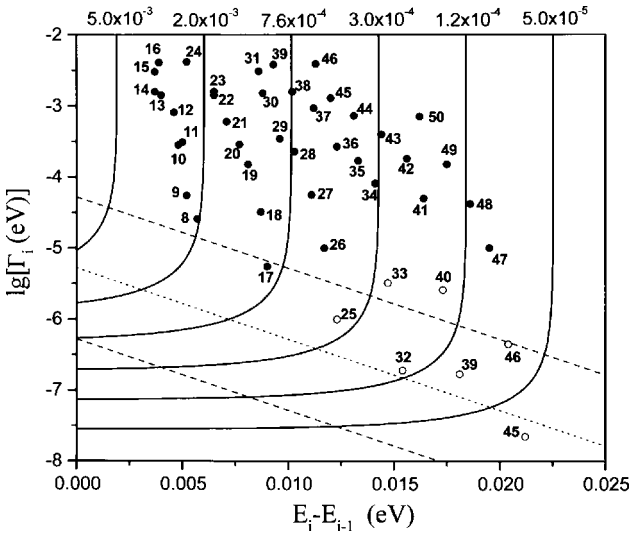

FIG. 6. Widths of *not* narrow resonances in our $O+O_2$ model. The SWP propagation and Prony analysis were used. Metastable states are labeled by the corresponding values of J. The dotted line corresponds to $\Gamma=k^s[M]$. Upper and lower dashed lines correspond to $\Gamma=10k^s[M]$ and $\Gamma=0.1k^s[M]$, respectively. The majority of the metastable states fall in the region $\Gamma \geqslant 10k^s[M]$ and should be assigned as broad. The contour map shows the value of $k_i^d k_i^s[M]/(k_i^d+k_i^s[M])$ which determines the contribution of a metastable state to the recombination rate. Empty circles show the metastable states with a large uncertainty in the SWP result for Γ. See text for details.

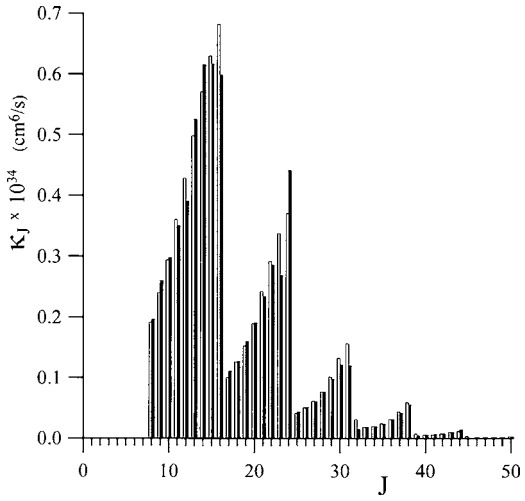

FIG. 7. Contributions $\kappa(J)$ of different J values to the total recombination rate of Eq. (44). Filled bars-SWP results; empty bars-WKB results. Transitions from maxima to minima occur every time the upper metastable state disappears due to centrifugal distortion of the potential (compare to Fig. 5).

into the intermediate regime. However, the states $J=17$ and 46 are so close to the upper dashed line that they can be treated as broad. The area below the lower dashed curve corresponds to $\Gamma_i \ll k^s_{i,(i-1)}[M]$ and all the narrow resonances fall into that area (not shown in Fig. 6), mainly outside of the figure frame. The contour lines in Fig. 6 show the value of $k_i^d k_i^s[M]/(k_i^d+k_i^s[M])$, which characterizes contributions of the metastable states to the total recombination rate κ. The seven most narrow resonances with large uncertainties in their Γ_i's (empty circles: $J=25$, 32, 33, 39, 40, 45, and 46) give the smallest contributions to κ and can be omitted for simplicity. Furthermore, two of these seven resonances, $J=33$ and 40, are broad according to criterion (38), so that their Γ_i's are not important.

Analysis of Figs. 5 and 6 shows that in our system all the important scattering resonances are either narrow or broad. The narrow resonances can be treated as bound states. The broad resonances contribute independently of the recombination rate and can be treated using Eq. (39) at every value of J. Finally, the total third order recombination rate coefficient (accumulated over all values of J) can be expressed as

$$\kappa = \sum_{J=0}^{\infty} \kappa(J) \approx \sum_J \sum_i K_i(J) k_i^s(J). \tag{44}$$

The equilibrium constants are obtained easily from statistical mechanics. For our pseudo-two-body model of $O+O_2$ collision [Eq. (4)] they should be calculated as[54]

$$K_i = \left(\frac{2\pi\hbar^2}{\mu k_B T}\right)^{3/2} (2J+1)\exp\{-E_i/k_B T\}. \tag{45}$$

All experimental and theoretical studies indicate that parameter ΔE in Eqs. (35) and (36) is quite small for the ozone forming reaction. In Ref. 55 it was determined as $\Delta E = 20 \pm 10$ cm^{-1}. Taking the value of $\Delta E = 20$ cm^{-1} and using the resonance energies calculated with SWP and WKB methods, we obtain for room temperature and pressure $\kappa^{SWP} = 4.91 \times 10^{-34}$ cm^6/s and $\kappa^{WKB} = 4.98 \times 10^{-34}$ cm^6/s, respectively. These numbers are very close to the experimental value of $\kappa^{expt} = 6.5 \times 10^{-34}$ cm^6/s reported in Ref. 3. Furthermore, if we use ΔE as a tuning parameter and attempt to fit κ^{expt} with κ^{SWP} by changing ΔE we obtain $\kappa^{SWP} = \kappa^{expt}$ at $\Delta E = 22.8$ cm^{-1}, which is within the error bars of the experimental result.

In these calculations the nitrogen gas (N_2) at a pressure of 1 atm was used as the third body M. For the majority of states shown in Fig. 6 the stabilization rate $k_i^s[M]$ varied in the range from 3×10^{-5} ps^{-1} (for $J=47$) up to 2×10^{-3} ps^{-1} (for $J=14$). Note that the dissociation rate coefficient was always larger: $k_i^d > 3 \times 10^{-3}$ ps^{-1}. The approach developed in this work is, nevertheless, very general and can be utilized in a wide range of concentrations $[M]$. We found, however, that the pressure dependence of κ is very weak, which also agrees with experimental data available for ozone forming reaction.[55] The effect of pressure on kinetics can be illustrated in a very clear way using the diagram of Fig. 6: If the pressure of the third body $[M]$ is reduced, the dashed lines in Fig. 6, which separate areas of stable and metastable states, are shifted down. As a result, some narrow resonances start contributing to the kinetics, whereas the contributions from the states with large Γ's decrease according to formula (33), so that the resultant κ remains roughly the same. In the opposite situation, when the pressure is increased, the border of stable and metastable states in Fig. 6 is shifted up into the area of larger Γ's, the number of truly metastable states drops (very narrow resonances stop contributing), but contributions from the broader resonances increase. This fully complies with results of Ref. 30.

Thus, the final results of two different semiclassical methods, κ^{SWP} and κ^{WKB}, are in very good agreement. Figure 7 shows the dependence of $\kappa(J)$ used in Eq. (44), and,

again, the results of SWP and WKB methods agree very well. At some values of J the SWP result slightly exceeds the result of WKB, while at other values of J the result of WKB is somewhat larger. But these differences compensate each other almost entirely when the sum (44) over all values of J is calculated.

V. CONCLUSIONS

In this work we demonstrated that the SWP method can be successfully applied to calculate energies and lifetimes of the metastable states trapped behind the centrifugal barrier. Such metastable states play a central role in many recombination reactions, including the ozone forming reaction. The model for the $O+O_2$ collision considered in this work was a simplified one: it does not describe all features of the PES and is not able to capture the anomalous isotope effects related to the multichannel nature of this reaction. However, this approximate model allowed us to carry out a thorough test of the method itself. Indeed, calculations of the scattering resonances are not easy for this system due to heavy masses of the nuclei, the deep potential energy well, and a broad centrifugal barrier. Despite these complications, the SWP method gave accurate predictions of energies for all under-the-barrier and over-the-barrier metastable states for all values of total angular momentum J. The lifetimes in the range of 0.5–100 ps, important for recombination reactions, were also accurately predicted. It is also quite encouraging that the SWP method was able to reproduce the experimental rate of ozone formation. Further development of this approach is ongoing, with the purpose to treat the ozone recombination reaction in full dimensionality, including associated isotope effects.

ACKNOWLEDGMENTS

Stephen Gray at Argonne is gratefully acknowledged for sharing his Prony code. This research was partially supported by the Petroleum Research Fund, Grant No. 43298-G6. It also used resources of the National Energy Research Scientific Computing Center, supported by the Office of Science of the U.S. Department of Energy under Contract No. DE-AC03-76SF00098. The authors would like to thank Professor Reid at Marquette University for his valuable help in preparation of the manuscript.

[1] J. Guenther, D. Krankowsky, and K. Mauersberger, Chem. Phys. Lett. **324**, 31 (2000).
[2] D. Krankowsky, F. Bartecki, G. G. Klees, K. Mauersberger, and K. Schellenbach, Geophys. Res. Lett. **22**, 1713 (1995).
[3] S. M. Anderson, D. Hülsebusch, and K. Mauersberger, J. Chem. Phys. **107**, 5385 (1997).
[4] F. A. Lindemann, Trans. Faraday Soc. **17**, 598 (1922).
[5] R. E. Roberts, R. B. Bernstein, and C. F. Curtiss, J. Chem. Phys. **50**, 5163 (1969).
[6] R. T Pack, R. B. Walker, and B. K. Kendrick, J. Chem. Phys. **109**, 6701 (1998).
[7] M. H. Thiemens, Science **283**, 341 (1999).
[8] K. Mauersberger, B. Erbacher, D. Krankowsky, J. Gunther, and R. Nickel, Science **283**, 370 (1999).
[9] J. Guenther, B. Erbacher, D. Krankowsky, and K. Mauersberger, Chem. Phys. Lett. **306**, 209 (1999).
[10] C. Janssen, J. Guenther, K. Mauersberger, and D. Krankowsky, Phys. Chem. Chem. Phys. **3**, 4718 (2001).
[11] K. Mauersberger, D. Krankowsky, C. Janssen, and R. Schinke, Adv. At., Mol., Opt. Phys. **50**, 1 (2005).
[12] B. C. Hathorn and R. A. Marcus, J. Chem. Phys. **111**, 4087 (1999).
[13] B. C. Hathorn and R. A. Marcus, J. Chem. Phys. **113**, 9497 (2000).
[14] B. C. Hathorn and R. A. Marcus, J. Phys. Chem. A **105**, 5586 (2001).
[15] Y. Q. Gao and R. A. Marcus, J. Chem. Phys. **116**, 137 (2002).
[16] Y. Q. Gao, W.-C. Chen, and R. A. Marcus, J. Chem. Phys. **117**, 1536 (2002).
[17] D. Charlo and D. C. Clary, J. Chem. Phys. **117**, 1660 (2002).
[18] T. A. Baker and G. I. Gellene, J. Chem. Phys. **117**, 7603 (2002).
[19] D. Babikov, B. K. Kendrick, R. B. Walker, P. Fleurat-Lesard, R. Schinke, and R. T Pack, J. Chem. Phys. **118**, 6298 (2003).
[20] D. Babikov, B. K. Kendrick, R. B. Walker, P. Fleurat-Lesard, R. Schinke, and R. T Pack, J. Chem. Phys. **119**, 2577 (2003).
[21] D. Babikov, B. K. Kendrick, R. B. Walker, R. Schinke, and R. T Pack, Chem. Phys. Lett. **372**, 686 (2003).
[22] H.-S. Lee and J. C. Light, J. Chem. Phys. **120**, 5859 (2004).
[23] R. Siebert, P. Fleurat-Lessard, M. Bittererova, S. C. Farantos, and R. Schinke, J. Chem. Phys. **116**, 9749 (2002).
[24] P. Fleurat-Lessard, S. Yu. Grebenshchikov, R. Siebert, R. Schinke, and N. Halberstadt, J. Chem. Phys. **118**, 610 (2003).
[25] R. Schinke, P. Fleurat-Lessard, and S. Yu. Grebenshchikov, Phys. Chem. Chem. Phys. **5**, 1966 (2003).
[26] R. Schinke and P. Fleurat-Lessard, J. Chem. Phys. **122**, 094317 (2005).
[27] R. Schinke, S. Yu. Grebenshchikov, M. V. Ivanov, and P. Fleurat-Lessard, Annu. Rev. Phys. Chem. **57**, 625 (2006).
[28] Y. Q. Gao and R. A. Marcus, Science **293**, 259 (2001).
[29] D. Babikov, R. B. Walker, and R. T Pack, J. Chem. Phys. **117**, 8613 (2002).
[30] R. T Pack and R. B. Walker, J. Chem. Phys. **121**, 800 (2004).
[31] E. J. Heller, J. Chem. Phys. **75**, 2923 (1981).
[32] M. F. Herman and E. Kluk, Chem. Phys. **91**, 27 (1984).
[33] E. Kluk, M. F. Herman, and H. L. Davis, J. Chem. Phys. **84**, 326 (1986).
[34] M. F. Herman, Chem. Phys. Lett. **275**, 445 (1997).
[35] V. S. Batista and W. H. Miller, J. Chem. Phys. **108**, 498 (1997).
[36] F. Grossmann, Phys. Rev. A **57**, 3256 (1998).
[37] K. G. Kay, J. Chem. Phys. **101**, 2250 (1994).
[38] Z. Li and R. B. Gerber, J. Chem. Phys. **99**, 8637 (1993).
[39] C. W. McCurdy and W. H. Miller, J. Chem. Phys. **67**, 463 (1977).
[40] S. Garashchuk and D. J. Tannor, Chem. Phys. Lett. **262**, 477 (1996).
[41] S. Garashchuk and D. J. Tannor, J. Chem. Phys. **110**, 2761 (1999).
[42] S. Garashchuk and J. C. Light, J. Chem. Phys. **114**, 1060 (2001).
[43] F. Grossmann, Chem. Phys. Lett. **262**, 470 (1996).
[44] D. Babikov, F. Aguillon, M. Sizun, and V. Sidis, Phys. Rev. A **59**, 330 (1999).
[45] V. A. Benderskii, E. V. Vetoshkin, and E. I. Kats, JETP **95**, 645 (2002).
[46] L. D. Landau and E. M. Lifshitz, *Quantum Mechanics: Non-Relativistic Theory* (Pergamon, New York, 1977).
[47] R. Sadeghi and R. T. Skodje, J. Chem. Phys. **99**, 5126 (1993).
[48] S. Marple, Jr., *Digital Spectral Analysis with Applications* (Prentice-Hall, Englewood Cliffs, 1987).
[49] S. K. Gray, J. Chem. Phys. **96**, 6543 (1992).
[50] C. Yang and S. K. Gray, J. Chem. Phys. **107**, 7773 (1997).
[51] See EPAPS Document No. E-JCPSA6-125-014625 which includes analysis of all scattering resonances in this system. This document can be reached via a direct link in the online article's HTML reference section or via the EPAPS homepage (http://www.aip.org/pubservs/epaps.html).
[52] J. Troe, J. Chem. Phys. **66**, 4745 (1977).
[53] R. G. Gilbert and S. C. Smith, *Theory of Unimolecular and Recombination Reactions* (Blackwell Scientific, Boston, 1990).
[54] R. T Pack, R. B. Walker, and B. K. Kendrick, J. Chem. Phys. **109**, 6714 (1998).
[55] H. Hippler, R. Rahn, and J. Troe, J. Chem. Phys. **93**, 6560 (1990).